Journal of Sound and Vibration (2003) **259**(5), 1011–1036
doi:10.1006/jsvi.2002.5160, available online at http://www.idealibrary.com on IDEAL®

TRANSIENT TURBULENT FRICTION IN SMOOTH PIPE FLOWS

A. E. Vardy and J. M. B. Brown

*Civil Engineering Department, University of Dundee, Dundee DD*1 4*HN, Scotland, UK.*
E-mail: a.e.vardy@dundee.ac.uk

(*Received* 17 *July* 2001*, and in final form* 11 *February* 2002)

A weighting function model of unsteady skin friction in smooth-walled, one-dimensional ducts is derived using an idealized form of the radial viscosity distribution. The model is an enhancement of earlier work by the authors in which additional simplifying assumptions were made. Important improvements include (1) replacing the assumption of uniform (solid) behaviour in an extensive core region by an assumption of uniform turbulent viscosity and (2) relating the wall shear stress to the mean flow velocity instead of to the maximum velocity. The resulting model can be used directly in numerical analyses of transient flows in pipes. It can also be used to deduce numerical values of an empirical coefficient in a popular alternative model of skin friction in which the unsteady contribution is assumed to be proportional to the instantaneous mean acceleration.

1. INTRODUCTION

The accurate prediction of the propagation of pressure wavefronts in pipes and tunnels is dependent upon the ability to model many phenomena that are secondary to the principal effect described by the Joukowski equation or the Rankine–Hugoniot equations. Secondary phenomena include, for example, cavitation and fluid–structure interaction, both of which can influence the evolving shapes of wavefronts as well as their amplitudes and speeds of propagation.

Another such phenomenon is skin friction. Historically, it has often been sufficient to represent skin friction in unsteady flows by quasi-steady models in which the resistance to flow at any instant is assumed to be equal to the resistance that would exist in a steady flow with the same mean velocity. This approach gives good agreement with experimental measurements when accelerations are sufficiently small—e.g., far from wavefronts in transient flows. Close to wavefronts, however, the influence of unsteady contributions to skin friction can be important. In particular, they influence the speed of propagation of wavefronts and the evolution of their spatial distribution (shapes). The purpose of this paper is to present a method of representing unsteady skin friction accurately in smooth-wall turbulent flows in pipes. It is hoped that ongoing work will lead in the near future to equivalent expressions for rough-wall turbulent flows.

Existing *one-dimensional* methods of representing unsteady contributions to skin friction may be classified into three groups, namely those based on instantaneous acceleration, those using past velocities/accelerations and those based on irreversible thermodynamics. The first of these has a long track record (e.g., references [1, 2]) and it is still the most popular method in software used for practical simulations. A recent description of the

0022-460X/02/$35.00

most commonly used model is given by Brunone *et al.* [3]. The magnitude of the unsteady component of skin friction is proportional to a coefficient k_3 whose value has to be determined empirically. Originally, values were deduced from experiments. More recently, use has been made of theoretically derived values provided by the authors [4]. The present paper improves these values and places their derivation on a sounder footing.

The second group of methods also has a long track record. They are based on an approach developed by Zielke [5] for laminar flows. The authors [4, 6] applied Zielke's methodology to an idealized model of turbulent flow in which the turbulent viscosity is assumed to vary linearly in an outer region of the flow (see section 2). This enabled approximate analytical solutions to be developed, leading to relationships for the decay of the wall shear stress following a sudden velocity change. The dependence of the Brunone *et al.* coefficient k_3 on the Reynolds number was deduced by applying both methodologies to a particular flow condition in which the two methods of analysis reduce to the same form.

The third group of one-dimensional methods is not considered in detail herein. Axworthy *et al.* [7] describe the current state of knowledge on the application of irreversible thermodynamics to unsteady skin friction in pipes. This approach has the advantage of a strong theoretical basis, but it nevertheless requires the values of empirical parameters to be deduced from experiment.

Two-dimensional methods have also been developed to describe unsteady skin friction. Examples include Ohmi *et al.* [8], Eichinger and Lein [9], Brunone *et al.* [10], Silva-Araya & Chaudhry [11] and Pezzinga [12]. These methods are able to provide much more detail than the one dimensional approaches, but they have the disadvantage of being unsuitable for general analyses of flows in extensive pipe networks. Today, they are best regarded as methods of advancing understanding and of assessing the validity of their one-dimensional counterparts, not as practical alternatives in their own right. This situation might change when computers become more powerful, but their understanding/validation roles may be expected to predominate for some years yet.

1.1. OUTLINE OF PAPER

The viscosity distribution used herein to represent turbulence in an unsteady pipe flow is presented in section 2 and compared with previous work. In section 3, it is used to deduce Laplace transforms of velocity profiles in an outer annulus of linearly varying viscosity and an inner core of uniform viscosity. This enables the derivation, in section 4, of an expression for the Laplace transform of the unsteady shear stress. The expression is too complex for an exact inverse transform to be found, but an approximate inverse is shown to be sufficiently accurate for practical purposes (section 5). This is used in section 6 to deduce values of the coefficient k_3 for use in instantaneous-acceleration formulae. Issues related to the practical usage of the methodology are discussed in section 7.

2. VISCOSITY DISTRIBUTION

The whole of the following development is based on two fundamental assumptions about the eddy viscosity, namely: (1) it has the piecewise linear form labelled "equations (1–3)" in Figure 1; and (2) it does not change during the period of interest.

The assumed distribution is defined in section 2.1 and the preceding assumptions are discussed in sections 2.2 and 2.3.

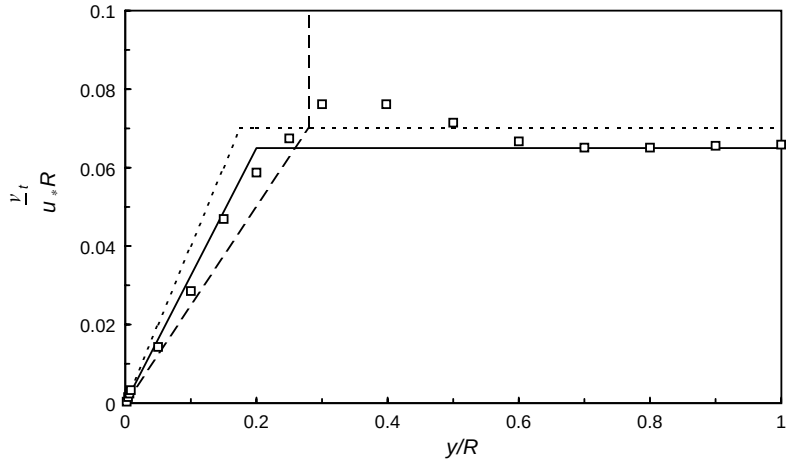

Figure 1. Comparison of idealized turbulent kinematic viscosity distributions with measurements by Laufer [13]. N.B. The intersection points used in this paper and by Ohmi [14] are fixed. The spatial location of the intersection point used previously by the authors [1, 5] varied with the Reynolds number. □, Laufer data [13]; — , Ohmi 2 region [14]; — — — —, Vardy and Brown [4]; ————, equations (1–3).

2.1. IDEALIZED DISTRIBUTION

In an annular region of width b adjacent to the wall, the viscosity is assumed to vary linearly from v_w at the wall to v_c at the interface between the annulus and an inner core region in which it is assumed to be uniform and equal to v_c. Later in the paper, the viscosity at the wall is assumed to be equal to the laminar kinematic viscosity, $v_{lam.}$ In the analytical development, however, it is written as v_w for compatibility with proposed future work in which it may not be equal to v_{lam}. The complete distribution may be written as

$$\left\{ \begin{array}{ll} annulus: & v = v_w(1 + \alpha y) \\ core: & v = v_c \end{array} \right\}, \tag{1}$$

where α, a fractional rate of change of viscosity with distance y from the wall, satisfies

$$\alpha = (v_c - v_w)/b v_w. \tag{2}$$

The co-ordinates of the intersection between the two regions are taken as

$$\sigma_c \equiv v_c/v_w = 0{\cdot}065\ u_* R/v_w, \qquad b = 0{\cdot}2\ R, \tag{3}$$

in which u_* is the friction velocity given by

$$u_* = \sqrt{\tau_w/\rho}, \tag{4}$$

where τ_w is the wall shear stress and ρ is the fluid density. A list of nomenclature is given in Appendix C.

2.2. JUSTIFICATION FOR THE ASSUMED VISCOSITY DISTRIBUTION

In Figure 1, the proposed viscosity distribution is compared with experimental evidence presented by Laufer [13] for steady, smooth-wall turbulent flow in a pipe. The idealization is somewhat coarse, but it captures the most important characteristic of the true distribution, namely a steady increase in the outer region close to the wall and an

approximately uniform viscosity in the core region. A very important benefit of the bi-linear approach is that it enables analytical solutions to be determined. More accurate idealizations would be likely to enforce the use of numerical methods of solution.

The chosen approximation is more realistic than the one used previously by the authors [4, 6]. In the earlier work: (1) both co-ordinates of the intersection point were different from equation (3) and indeed, the width of the annulus was allowed to vary with the Reynolds number; (2) the core region was treated as though it were a solid (i.e., it had infinite viscosity).

Even with these coarse assumptions, the previous method led to results that have been used by other authors with some success (see section 7.2). That is, predicted pressure histories have been found to compare favourably with experimentally measured ones. This suggests that the underlying ideas in the earlier work are sound and hence that they may usefully be developed in a more rigorous manner.

For completeness, the previously assumed distribution is included schematically in Figure 1 together with an approximation used by Ohmi and Usui [14].

2.3. JUSTIFICATION FOR AN INVARIANT VISCOSITY DISTRIBUTION

Attention now turns to the assumption that changes in the viscosity distribution may be neglected during the transient flow process. This assumption *cannot* be valid over large time scales because the flow must adjust to the evolving conditions. In a step change from one steady state mean velocity to another, for instance, the initial and final viscosity distributions must be those of the initial and final flow rates.

Suppose that the step change in velocity occurs suddenly. At early times after the transient, the change in velocity remote from the wall will be very nearly equal to the change in the mean velocity and there will be negligible changes in velocity gradients. As time increases, however, vorticity diffusion from the wall towards the pipe axis will have increasing influence, gradually changing the velocity profile to the shape appropriate for steady flow with the new mean velocity. The change in the effective viscosity occurs during the period when the *shape* of the velocity profile is changing, not during the earlier period when the velocity amplitude increases uniformly. That is, there is a phase lag between the step change in mean velocity and the resulting change in the effective viscosity.

The time interval between the step change in velocity and the arrival of significant vorticity diffusion reduces with increasing radius. At the wall itself, the interval is nominally zero because the no-slip condition requires that the velocity is always zero. At this extreme location, however, the viscosity is wholly laminar and so remains permanently unchanged. That is, there is no radius at which the effective viscosity changes significantly in the early stages after the passage of the step in velocity.

There is strong supporting evidence for the above description. He and Jackson [15] reported an extensive series of experiments with ramp changes in velocity (increases and decreases) over various time periods. They identified three separate time scales and confirmed the slug flow nature of the initial response in the core region. They also showed that the viscosity in the outer region does not respond as rapidly as the local velocity gradients. On the contrary, there is little increase in turbulence in the outer zone until the influence of the increased velocity gradients has extended radially inwards to the region where turbulence production peaks. Their results are consistent with earlier studies by Maruyama *et al.* [16].

There is also strong theoretical evidence. Ghidaoui *et al.* [17] studied alternative models of radial viscosity distributions. They reached two conclusions of importance for the

present paper. First, they confirmed that the time scales required for the shapes of the velocity distributions to respond to changes to the mean flow are far greater than those required for wavefronts to travel similar distances. Second, they found that predictions of the overall flow were not sensitive to small variations in assumed viscosity distributions. This second conclusion implies that the differences shown in Figure 1 between the bi-linear viscosity distribution and experimental measurements should be unimportant for present purposes.

It follows from the above evidence that (1) the assumption of an initially unchanged viscosity distribution is reasonable, but that (2) it cannot be accurate over timescales comparable with those needed for significant vorticity diffusion to reach the pipe axis from the wall. These factors place upper and lower bounds on the times for which the theoretical model in this paper is valid. For completeness, however, note that inaccuracies in the later stages of the flow change will be important only if the changes in effective viscosity are significant. For example, they will be important in the case of a sudden change from rest to steady velocity, but they might be less important in a change of equal magnitude from a large steady velocity to a slightly larger one.

In the preceding discussion, it is assumed that a steady flow is disturbed by a single transient. At sufficiently small times after the transient, the governing viscosity distribution corresponds to the initial steady flow. In more general flows, however, the transient might occur at an instant when the flow is already unsteady. In this case, the appropriate initial viscosity distribution will correspond to an unsteady flow state and will not be known *a priori* by the analyst. This difficulty is disregarded in the following development, but it is discussed in section 7.

3. VELOCITY PROFILE AND VOLUME FLOW RATE

The first step in the analytical development is the determination of velocity profiles in the annulus and core regions and the use of these to obtain a relationship between pressure gradients and velocity changes. This process is summarized here and is presented in detail in Appendix A.

Independent co-ordinate systems are used in the two regions (see Figure 2). In the outer annulus, planar co-ordinates are used with the y-axis facing radially inwards from the wall. In the core region, cylindrical polar co-ordinates are used. In both cases, the axial co-ordinate is x.

The momentum and continuity equations of one-dimensional incompressible flow yield the following equations in the annulus and in the core:

$$\frac{\partial u}{\partial t} = -P + \frac{\partial}{\partial y}\left(\nu(y)\,\frac{\partial u}{\partial y}\right) \tag{5}$$

and

$$\frac{\partial u}{\partial t} = -P + \frac{\nu_c}{r}\,\frac{\partial}{\partial r}\left(r\,\frac{\partial u}{\partial r}\right), \tag{6}$$

where ν, the kinematic turbulent viscosity, varies with y in the annulus, but is constant in the core region, and

$$P \equiv \frac{1}{\rho}\,\frac{\partial p}{\partial x} - \frac{\mathrm{d}Z}{\mathrm{d}x}, \tag{7}$$

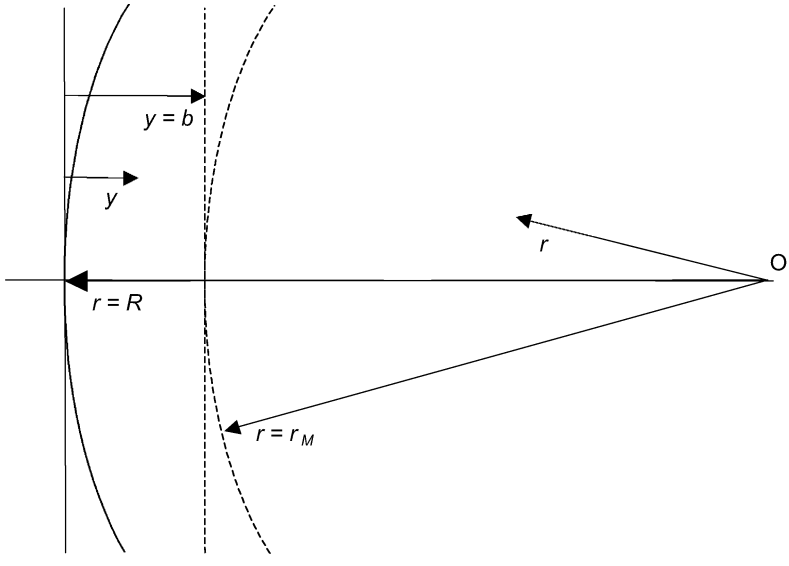

Figure 2. Co-ordinate systems in the annulus and the core.

in which p is the fluid pressure, ρ is the fluid density and Z is a body force potential (e.g., gravitational). Herein, P is regarded as a prescribed quantity; it is loosely referred to as a driving force.

Equations (5) and (6) can be converted into ordinary differential equations by means of the Laplace transform and can then be integrated subject to appropriate boundary conditions. In the following development, transformed parameters are denoted by a prime ($'$) and the Laplace transform variable is denoted by s. Herein, s is real, not complex.

Initially, the integration proceeds independently in the annulus and the core. Matching conditions are then imposed at the interface between these regions to yield a self-consistent velocity distribution over the whole cross-section. Using the suffices MA and MC to denote the matching point in the annulus and core, respectively, the boundary conditions for the initial phase are

$$\left\{\begin{array}{lll} annulus: & u_{y=0} = 0, & u_{y=b} = u_{MA} \\ core: & (\partial u/\partial r)_{r=0} = 0, & u_{r=R-b} = u_{MC} \end{array}\right\}, \tag{8}$$

and the matching conditions are

$$u_{MA} = u_{MC} \equiv u_M, \quad \tau_{MA} = \tau_{MC}. \tag{9}$$

Since the viscosity is continuous at the interface, the second of these conditions may be interpreted as requiring the equality of $(\partial u/\partial y)_{MA}$ and $-(\partial u/\partial r)_{MC}$. The minus sign arises here because the axes y and r are in opposite directions.

It is shown in Appendix A that the Laplace transforms of the resulting velocity distributions in the two regions may be expressed as (see equations (A21) and (A24) in Appendix A)

$$u'(\eta) = [C_1 \mathrm{I}_0(\eta) + C_2 \mathrm{K}_0(\eta) - 1](P'/s) \tag{10}$$

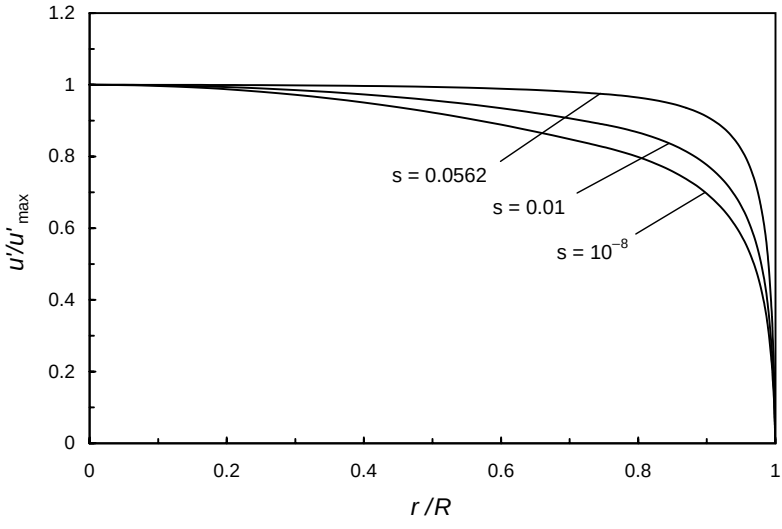

Figure 3. Evolution of the transformed velocity following the sudden application of a pressure gradient ($v_w = 15\,\mathrm{mm}^2/\mathrm{s}$, $\sigma_c = v_c/v_w = 101$).

and

$$u'(r) = \left(\frac{(1+H)\ \mathrm{I}_0\ (r\sqrt{s/v_c})}{\mathrm{I}_0(r_M\sqrt{s/v_c})} - 1 \right) \frac{P'}{s}, \tag{11}$$

in which η is a non-dimensional distance co-ordinate defined by equation (A2) in Appendix A. The coefficients C_1 and C_2 are dependent on the parameter H, which is defined by equation (A19) in Appendix A and which relates the velocity at the interface to the "driving force" P'/s. The expressions I_0 and K_0 are, respectively, modified Bessel's functions of the first and second kinds and zero order.

Figure 3 shows typical (transformed) velocity profiles following a step change in the mean velocity. Profiles are shown for three values of the Laplace transform variable s and each is non-dimensionalized with respect to its own maximum velocity. This highlights the evolving shape of the profile from the early flattish form to the final profile shown by the curve $s = 10^{-8}$ (NB: small values of s correspond to large values of real time t).

In section 2.3, it was shown that the assumption of a "frozen" viscosity distribution is reasonable in the early stages after a transient event, but that it is not correct in later stages. An inevitable consequence is that predictions for very large times will be incorrect. In Figure 3, the curve labelled $s = 10^{-8}$ will be a false asymptote because it assumes that the original viscosity distribution has survived the change in velocity. Given sufficient time, the true flow would evolve to a different asymptotic condition consistent with its own viscosity distribution. Nevertheless, the early stages of the predicted evolution should be reliable. This is the period when the greatest unsteady components of wall shear stress are expected.

3.1. MEAN VELOCITY

The flow rates in the annulus and the core can be determined by integrating the velocity profiles and their sum can be used to determine a mean velocity, which satisfies

$$GU' = P'/s, \tag{12}$$

where G is given by equation (A29) in Appendix A. The flow rate in the core is determined by exact integration of equation (11). The flow rate in the annulus is determined in an approximate manner that is shown in the appendix to imply negligible error.

4. THE WALL SHEAR STRESS

In Appendix A, the total wall shear stress τ_w is obtained by differentiating the velocity distribution in the annulus and using $\tau_w = \rho v_w (\partial u/\partial y)_{w.}$ The stress is regarded herein as the sum of two components, namely

$$\tau_w = \tau_{ws} + \tau_{wu}, \tag{13}$$

where τ_{ws} and τ_{wu} are contributions from the steady and unsteady components of flow respectively.

To deduce the unsteady contribution $\tau_{wu,}$ it is necessary to subtract τ_{ws} from τ_w. This requires the development of steady-flow relationships in the same form as the preceding equations. The necessary development is presented in Appendix B, following the same sequence as that used for the general flow. By subtracting the steady-flow expression from the general expression and using (for zero initial velocity)

$$sU' = \left(\frac{\partial U}{\partial t}\right)', \tag{14}$$

the Laplace transform of the unsteady contribution to the wall shear stress can be expressed as

$$\frac{\tau'_{wu}}{\rho v_w} = \frac{\Phi_u}{s}\left(\frac{\partial U}{\partial t}\right)', \tag{15}$$

where Φ_u is a transfer function between the transforms of the mean velocity and the unsteady component of the wall shear stress. It satisfies

$$\Phi_u = \sqrt{\frac{s}{v_w}}[C_1 \mathrm{I}_1(\sqrt{\zeta}) - C_2 \mathrm{K}_1(\sqrt{\zeta})]\; G - \frac{1}{\alpha v_w}\left[1 - \sigma_c - \frac{\alpha r_M}{2}\right] G_s, \tag{16}$$

where G_s is the steady-flow equivalent of G. The expressions I_1 and K_1 are, respectively, modified Bessel's functions of the first and second kinds and first order. The inverse transform of equation (15), derived in section 5, provides the required dependence of the unsteady component of the shear stress on the flow history.

4.1. RELEVANCE OF THE UNSTEADY COMPONENT OF SHEAR STRESS

In engineering practice, it is unlikely that the *unsteady* component of the wall shear stress will be important in its own right. It is more likely that an analyst will wish to know the total shear stress. This may be evaluated by calculating the unsteady component as described herein and adding it to an independently estimated value of the steady-flow component. Typically, the latter will be obtained from well-known expressions for steady

flows in pipes (e.g., the Darcy Weisbach equation together with a smooth-wall relationship for the quasi-steady skin friction coefficient).

It is instructive to ask why effort is devoted to subtracting the steady-flow contribution in the above development and thereby requiring writers of software to add it back in again. There are several reasons for this, but two are especially important. First, the characteristic behaviours of the steady and unsteady components are different and this is reflected in their mathematical representation. As a consequence, even if both components were retained, it would be necessary to handle them independently.

A more important reason is that the separated approach is potentially more accurate. The method used herein to represent the turbulent flow is based on an idealized viscosity distribution. This is true of quasi-steady contributions to velocity profiles as well as to unsteady contributions. It is highly likely that well-established methods of predicting quasi-steady shear stresses in pipe flows will be more accurate than a method based on an idealized distribution. Accordingly, it is rational to enable purpose-designed steady-flow methods to be used to estimate quasi-steady contributions to the shear stress.

In principle, the second argument would also apply to the unsteady contribution if accurate alternative methods were available. In practice, however, this happy state of affairs does not prevail. The method presented herein is expected to be more accurate than any current alternative.

4.2. COMPARISON WITH PREVIOUS WORK

For completeness, it is worth noting that equation (15) differs in an important respect from the equivalent expression in the authors' previous work [4, 6]. The equation relates the transforms of the wall shear stress and the mean velocity whereas the earlier work related the transforms of the wall shear stress and the (uniform) core velocity. In the earlier work, this led to an incompatibility which, although recognized and stated, was neglected. No such incompatibility exists in the present development.

5. THE WEIGHTING FUNCTION

The inverse Laplace transform of equation (15) can be expressed as a convolution

$$\tau_{wu} = \frac{2\rho\nu_{lam}}{R}\int_0^T W\frac{\partial U}{\partial t}\,\mathrm{d}t^*, \tag{17}$$

in which R is the radius of the pipe, T is the elapsed time since the beginning of the unsteadiness and $t^* = T - t$ is backward-measured time from the instant at which the integral is being evaluated. The weighting function W is a function of t^* whereas the acceleration $\partial U/\partial t$ is a function of t. The factor of 2 on the right-hand side is introduced for compatibility with the weighting function derived by Zielke [5] for unsteady *laminar* flow.

The Laplace transform of equation (17) is

$$\tau'_{wu} = \frac{2\rho\nu_{lam}}{R}\,W'\left(\frac{\partial U}{\partial t}\right)' \tag{18}$$

and so, by comparison with equation (15), the transformed weighting function satisfies

$$W' = \frac{R}{2}\,\frac{v_w}{\nu_{lam}}\,\frac{\Phi_u}{s}. \tag{19}$$

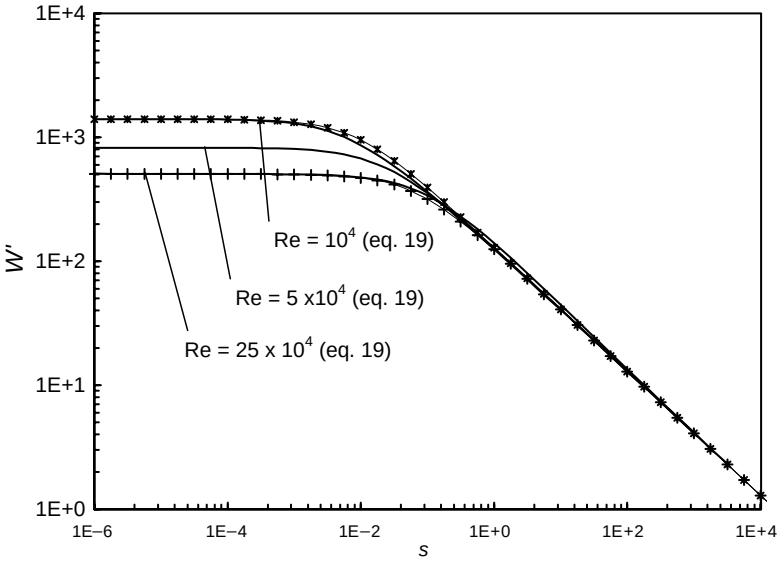

Figure 4. Transformed weighting function and its approximation. The markers denote the approximate weighting function, equation (20).

The continuous lines in Figure 4 show the weighting function transform for three values of the core viscosity. All three curves approach the same asymptote at sufficiently large values of s (i.e., at sufficiently small times), but they approach different constant asymptotes at small s (large time). This behaviour is a consequence of the characteristic response of a flow to an imposed change to the mean velocity. The first response is felt at the wall where, for smooth-pipe flows, $v = v_{lam}$ irrespective of the viscosity elsewhere. Later, when radial vorticity diffusion has carried the response to the disturbance further from the wall, the weighting function is influenced by the viscosity distribution.

5.1. APPROXIMATE WEIGHTING FUNCTION, W_a

In his laminar-flow analysis, Zielke [5] undertook the inverse transform analytically to obtain an exact expression for the weighting function W in the form of an infinite series. The result cannot be used conveniently in numerical analyses, but Zielke showed that it can be approximated by simpler expressions that can be used easily. He derived simple approximations for use (1) at very small times and (2) at larger times.

Herein, a different approach is used. An approximation is introduced *before* the inverse transform is obtained. That is, the transformed weighting function is approximated by a much simpler function that has almost the same form and for which a simple inverse exists. A big advantage of this approach is that it leads to a convenient analytical expression for the weighting function. Moreover, the expression is valid for all times, large and small. The approximation in the Laplace transform plane is

$$W'_a = A/\sqrt{s + B}, \tag{20}$$

in which the suffix "a" indicates that the weighting function is approximate. The values of the parameters A and B are chosen to ensure that the approximation is exact at both asymptotes of s. Figure 4 compares the true and approximate functions.

The value of the parameter A is determined by matching the asymptotic states of equations (19) and (20) at large s. In this case, W_a' tends to $A/\sqrt{s}$ and the asymptotic matching process yields

$$A = R\sqrt{v_w}/2v_{lam}. \tag{21}$$

When s is very small, W_a' tends to $A/\sqrt{B}$. The authors have been unable to obtain an analytical expression for the corresponding asymptotic value of W' and so, as a practical way forward, values are obtained numerically for any particular curve. Denoting such a value by W_0', the matching process for very small s yields

$$B = (A/W_0')^2. \tag{22}$$

By using these expressions for A and B, the inverse transform of equation (20) can be expressed as

$$W_a = \frac{\sqrt{(v_w/v_{lam})}\,\exp(-\psi/C^*)}{2\sqrt{\pi\psi}}, \tag{23}$$

in which ψ is the non-dimensional time and C^* is the shear decay coefficient that is a function of the Reynolds number. These parameters are defined by

$$\psi \equiv v_{lam}t^*/R^2 \quad \text{and} \quad C^* \equiv v_{lam}/BR^2. \tag{24}$$

The most important difference between this result and the corresponding one in the authors' previous work [4] arises from the implied numerical values of the parameter C^* (see section 5.2). A lesser difference is the inclusion of the ratio v_w/v_{lam} in equation (23). Herein, this ratio is equal to unity.

Figure 5 shows the predicted weighting functions for a range of Reynolds numbers, using both log–log and natural scales. Zielke's laminar-flow weighting function [5] is shown for comparison. By inspection, the greatest values of the weighting function occur at small times, thereby coinciding with the period when the assumption of a frozen viscosity distribution (see section 2) is most reasonable. At larger times where the assumption is least reasonable, the magnitudes of the weighting functions are much smaller. In practical numerical simulations, this implies that the influence of a step change in the mean velocity will be estimated most accurately immediately after it occurs; significant inaccuracies will arise only after the influence of the step change has reduced.

5.2. NUMERICAL EVALUATION OF C^*

In the absence of further development, the need to include the numerically derived asymptote W_0' in the expression for B would detract greatly from the practical utility of the proposed weighting function. To circumvent this need, the above process has been repeated many times (using a spreadsheet) to determine values of B (and hence C^*) for a wide range of Reynolds numbers. A regression analysis has then been used to express the collective results as a relationship between C^* and the Reynolds number $\mathbf{Re}$. Over the range $2000 < \mathbf{Re} < 10^8$, C^* is found to satisfy closely

$$C^* = 12{\cdot}86/\mathbf{Re}^{\kappa}, \tag{25}$$

in which

$$\kappa = \log_{10}\left(\frac{15{\cdot}29}{\mathbf{Re}^{0{\cdot}0567}}\right). \tag{26}$$

The greatest difference between values obtained by using these expressions and the numerically derived values of C^* over the specified range is less than 0·2%. The value of

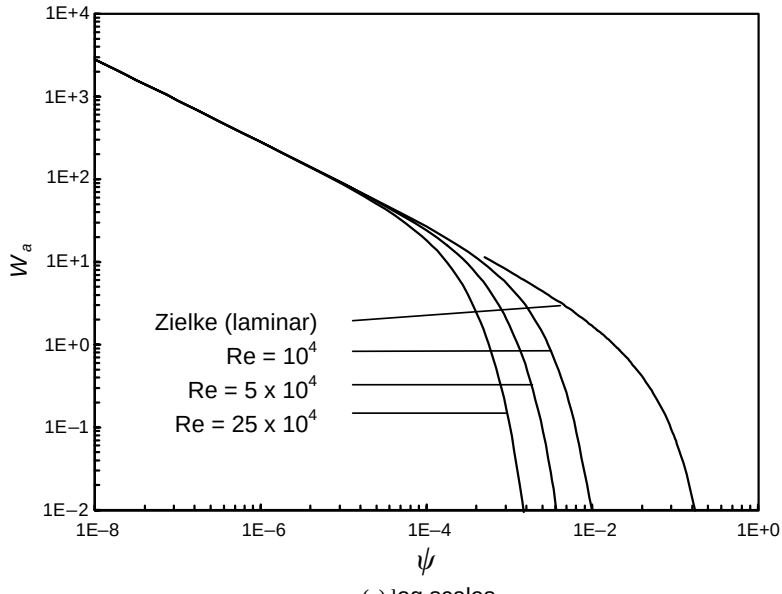

(a) log scales

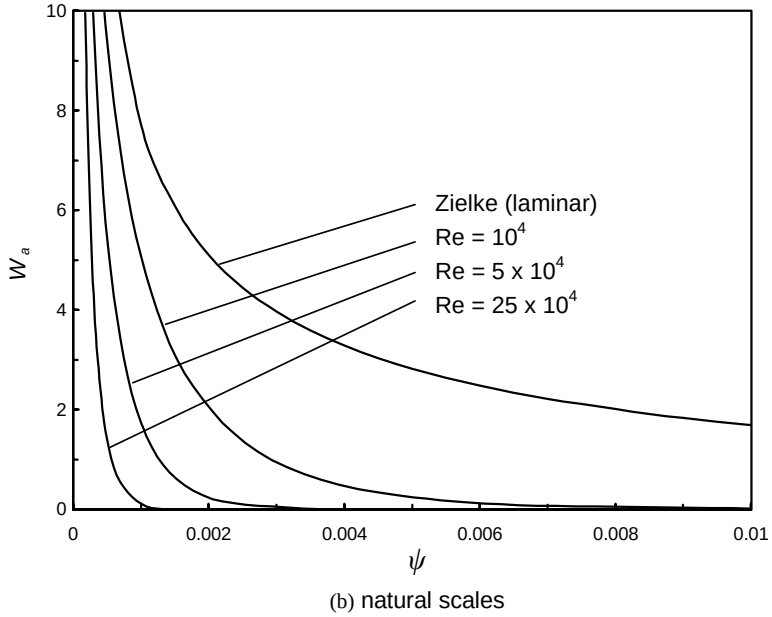

(b) natural scales

Figure 5. Approximate weighting functions.

C^* varies rapidly at small values of **Re**, but less rapidly at large values. Its dependence on **Re** is illustrated in Figure 6 which also shows the corresponding values of C^* obtained using the authors' 1995/6 model with a uniform velocity core region. The present values are larger, showing that the previous model overestimated the rates of decay, especially at large Reynolds numbers. That is, the influence of unsteady skin friction persists for longer than was previously predicted.

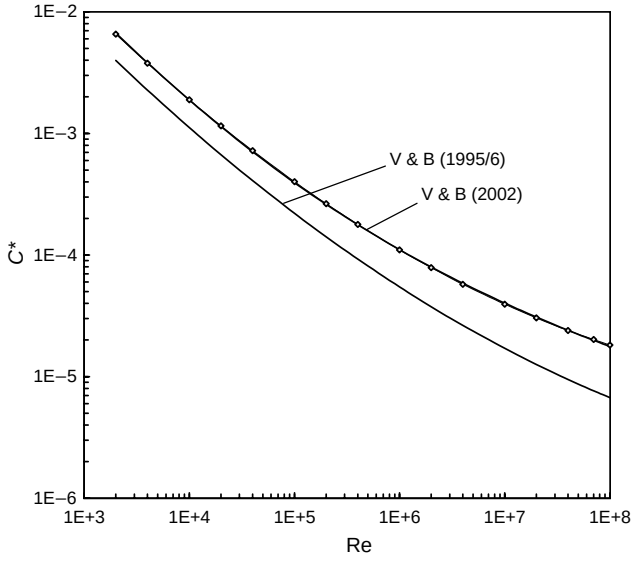

Figure 6. Reynolds number dependence of the shear decay parameter C^*. The markers denote the interpolated function given by equations (25) and (26).

6. UNSTEADY FRICTION COEFFICIENTS

6.1. LIMITING SHEAR STRESS

Valuable information about unsteady shear stresses can be obtained by considering the special case of a uniform acceleration $\dot{U}_0 = \partial U/\partial t$. By using the approximate weighting function (equation (23)), the shear stress relationship (equation (17)) can be integrated to give an unsteady friction coefficient f_u as

$$f_u \equiv \tau_{wu}/\tfrac{1}{2}\rho \dot{U}_0 R \approx 2\sqrt{C^*}\ \mathrm{erf}(\sqrt{\psi_T/C^*}), \tag{27}$$

in which erf( ) is an error function and ψ_T is the non-dimensional elapsed time since the acceleration began (it corresponds to the time T).

For any particular **Re**, the shear decay coefficient C^* is constant and so the error function determines the shape of the unsteady shear stress history. Figure 7 illustrates the development during a uniform acceleration from initial Reynolds numbers of 10^5 and 10^7. The error function is zero when $\psi_T = 0$ and it approaches unity asymptotically as $\psi_T \to \infty$. Therefore, the unsteady friction coefficient approaches a limiting (asymptotic) value of

$$f_{uL} = 2\sqrt{C^*}. \tag{28}$$

The figure also shows the corresponding predictions when using the value of C^* obtained for the solid core model used in the 1995/6 analysis. By inspection, the two models yield similar results at very early times, but they diverge with increasing time as the core region begins to exert an influence.

In common with all of the development so far, Figure 7 is based on the assumption of a frozen viscosity distribution (see section 2). As a consequence, the limiting value f_{uL} may be regarded as a property of the particular viscosity distribution. Since the latter is a function of the Reynolds number, it follows that f_{uL} is itself a function of the Reynolds number—as equations (25) and (28) show. The dependence is illustrated in Figure 8, which

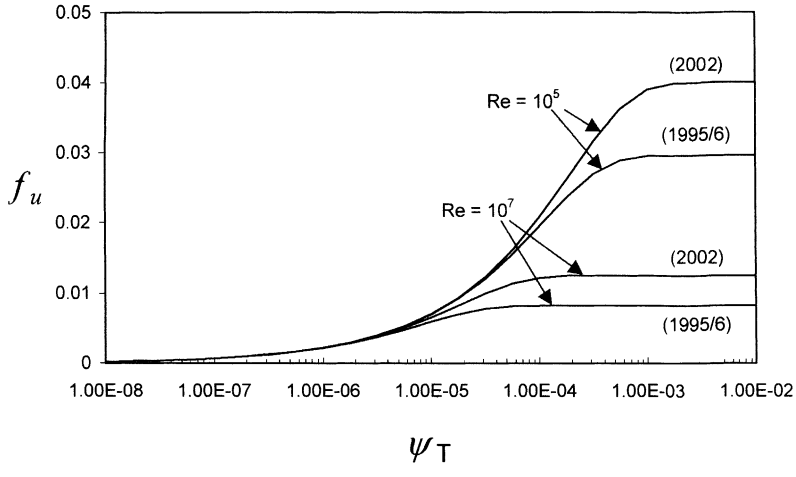

Figure 7. Growth of the unsteady skin friction coefficient during uniform acceleration.

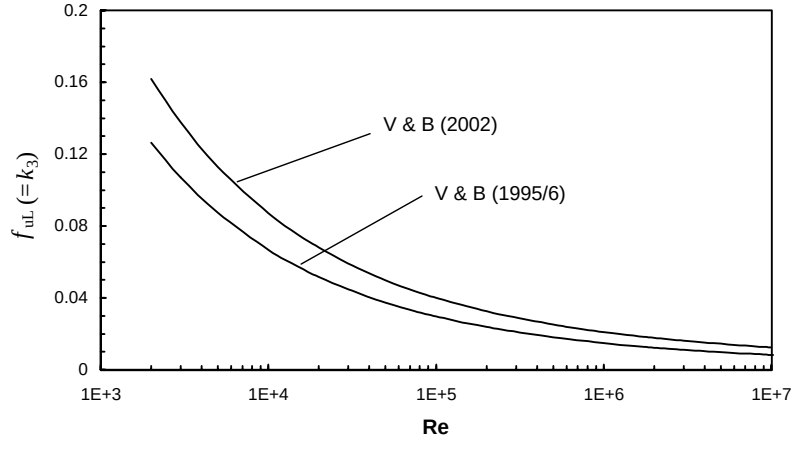

Figure 8. Reynolds number dependence of the limiting unsteady skin friction coefficient (and hence of Brunone's coefficient k_3).

also shows the corresponding predictions for the previous model [5]. The current values are larger, typically by about 30%.

Figure 8 can be used to estimate upper and lower bounds to the actual value of the unsteady shear stress in a uniformly accelerating flow. Suppose, for example, that the mean flow accelerates uniformly from a steady value of $\mathbf{Re}_1$ to a larger value $\mathbf{Re}_2 > \mathbf{Re}_1$. If the acceleration is rapid, the unsteady shear stress coefficient might be well approximated by the early part of Figure 7, rising continuously, but always less than the limiting value. That is, the upper bound to possible values of f_u during the acceleration is $f_{uL}(\mathbf{Re}_1)$. In contrast, if the acceleration time scales are long in comparison with vorticity time scales (see section 2.3), the instantaneous values of f_u might correspond closely to $f_{uL}(\mathbf{Re})$ where **Re** denotes the instantaneous value of the Reynolds number. Since f_{uL} decreases when **Re** increases, it follows that the lower bound to possible values of f_u is $f_{uL}(\mathbf{Re}_2)$.

Another useful conclusion can be drawn from Figure 8. The decreasing amplitude of f_{uL} with increasing Reynolds number shows that the magnitudes of unsteady skin friction

forces will tend to decrease with increasing Reynolds number. Since the opposite is true for quasi-steady shear stresses, it is clear that, for any particular acceleration $\dot{U}_0$, the *relative* importance of unsteady skin friction will decrease rapidly as **Re** increases. This is consistent with experimental data such as that reported by Holmboe and Rouleau [18].

Notwithstanding the qualitative trends identified in the preceding paragraph, the absolute amplitude of the unsteady shear stress depends upon the acceleration $\dot{U}_0$, as well as upon f_u. With sufficiently large accelerations, unsteady skin friction can dominate quasi-steady skin friction even at large Reynolds numbers. This is the case, for example, close to steep wavefronts caused by events such as rapid valve closure. Consider, for instance, a classical waterhammer situation in a pipeline with a large length : diameter ratio. At any particular location, the phenomenon will be characterized by long periods of quasi-steady flow punctuated by sudden events when a wavefront passes. It is reasonable to expect that unsteady skin friction will continually dissipate the individual wavefronts, but that quasi-steady forces might be more important than unsteady skin friction in the long periods between wavefronts.

6.2. INSTANTANEOUS-ACCELERATION FORMULAE

One reason for considering uniform accelerations is that it enables the weighting function approach to provide information required in instantaneous-acceleration formulae for unsteady skin friction. It was shown by Vardy and Brown [4] that, for the particular case of uniform acceleration, the parameter k_3 used by Brunone *et al.* [3, 19] is equal to f_{uL}. As a consequence, the method described above to evaluate f_{uL} may also be interpreted as a method of evaluating k_3. For any particular Reynolds number, this gives a unique value for k_3 even though the unsteady shear stress (and hence the unsteady friction coefficient f_u) is not constant. The general shape of these curves is similar to that found for smooth pipes by Pezzinga [12] for his parameter k_2, which is closely related to Brunone's k_3.

For reasons discussed in section 6.1, there is some ambiguity in the determination of the most appropriate value of f_{uL} for any particular Reynolds number. That is, the most appropriate value is dependent on the acceleration as well as upon the Reynolds number. However, the logic that led to this conclusion also applies to the parameter k_3. That is, this parameters should also be dependent upon the acceleration. Moreover, the general trends should be the same for both parameters. As a consequence, it seems reasonable to suppose that a reasonable estimate for k_3 at any particular value of **Re** will be obtained by estimating the asymptotic value f_{uL} for the same Reynolds number.

6.3. RISE TIMES

The limiting value of f_u is approached asymptotically as time increases. In standard tables (e.g., reference [20]), the error function is shown to attain a value of 0·99 at an argument of 1·823. Using this as an effective limit, it follows from equation (27) that the non-dimensional time required to reach the limiting shear stress is

$$\psi_{TL} = 3{\cdot}323C^*. \tag{29}$$

This is the same expression as the one given by Vardy and Brown [4]. However, the implied numerical values of ψ_{TL} for any particular Reynolds number are greater than those in the earlier paper because of the new values in equations (25) and (26). This is shown in Figure 9.

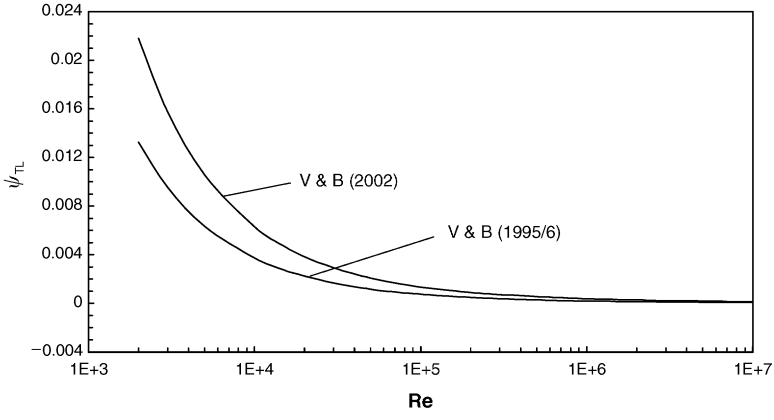

Figure 9. Reynolds number dependence of the time to approach limiting unsteady shear stress conditions.

Physically, the rise time is related to the time required for vorticity diffusion over the cross-section. In simulations of waves in pipes, ducts and tunnels, it can usefully be compared with the times required for waves to develop (valve closure times, etc.) and for waves to propagate through the system (see reference [17] for example).

7. USE OF THE WEIGHTING FUNCTION MODEL

Three approximations have been made in the preceding development, namely; the turbulent viscosity distribution has been represented in a bi-linear manner; no account has been taken of time-variations in the viscosity distribution; and a Cartesian co-ordinate system has been used in the annulus region.

In principle, all three of these approximations have the potential to invalidate the use of the model. It is therefore appropriate to explore their influence carefully. In practice, this is best done by appealing to experimental evidence (see section 7.2). First, however, special attention is paid to some consequences of the second assumption for practical applications in numerical analysis.

7.1. SELECTION OF THE VISCOSITY DISTRIBUTION

It was pointed out in section 2 that ambiguity can arise in the selection of the "initial" flow condition on which the viscosity distribution is based. In some cases, the choice is obvious, but in others, it is less clear.

Consider the special case of a step change in velocity from one steady value to another. In this case, the relevant viscosity distribution is the one in the initial steady flow. Considerable time will elapse before the whole velocity profile adjusts to the new steady state condition, but the unsteady shear stress will be important only during the early stages of this process. That is, although the assumed viscosity distribution will become increasingly unrealistic as time increases, its influence on the numerical predictions will become successively smaller.

It is possible to invoke experimental evidence from reference [21] in support of this argument. Arlt undertook experiments in which a flow was suddenly accelerated from rest to a steady velocity. He showed that the measured values of the unsteady skin friction were

well approximated by predictions based on Zielke's laminar-flow analysis. Hitherto, this evidence has been interpreted as implying that the laminar flow formulae are approximately valid in turbulent flows too. With the benefit of hindsight, however, it is now asserted that the experiments demonstrate only the importance of the initial viscosity distribution.

Now consider more general flows in which the choice of the initial viscosity distribution is not obvious. This is the case in many practical simulations of transient flows. For such analyses, the spirit of the above discussion implies that the most appropriate *steady-flow* viscosity distribution for use at any instant would be one corresponding to conditions at some earlier time. In the absence of other information, use might be made of equation (29) to define the time interval. A simpler, alternative would be to base the viscosity distribution on the most recent available velocity. Indeed, this might be the only practicable option in numerical methods of solution where all information before the current calculation time is discarded as the solution proceeds. If such an analysis uses the instantaneous-acceleration parameter k_3 and approximates it by $f_{uL}(\mathbf{Re})$, the result will be as described in section 6.1.

7.2. EXPERIMENTAL AND THEORETICAL EVIDENCE

Independent theoretical evidence can be used to confirm the approximate validity of the weighting functions presented herein. For example, Ghidaoui and Mansour [22] compare alternative predictions of pressure histories in a waterhammer experiment. For present purposes, the most important conclusion from their study is that predictions based on the authors' weighting function [6] agree closely with those based on a two-dimensional turbulence model proposed by Pezzinga [23].

Further theoretical evidence is provided by Zarzycki [24, 25], who develops a weighting function model using a four-region discretization of the turbulent viscosity distribution. The core region is modelled in the same manner as the present paper, but there are three outer zones instead of just one. Graphical comparisons are presented to show that the authors' weighting function [4] underestimates the unsteady component of shear stress, especially at high Reynolds numbers. This conclusion is consistent with the predictions reported herein. Moreover, the magnitudes of the predicted differences are broadly similar to those obtained herein.

There is no direct *experimental* evidence of the validity of the weighting functions. There is, however, *indirect* evidence through comparisons of measured pressure histories with numerical predictions using instantaneous-acceleration models of unsteady skin friction. Bergant *et al*. [26] obtained experimental measurements of transient flows induced by valve closure in a pipeline. Three different pre-existing steady flows were considered and comparisons were made with predictions based on alternative values of the parameter k_3. The best-fit value of k_3 was found to agree closely with values obtained for f_{uL} from reference [4].

Although not stated explicitly, it is surmised that the value of k_3 used by Bergant *et al*. was invariant during each waterhammer simulation. Subsequently, Vitkovsky *et al*. [27] showed that results obtained using variable values of k_3—based on the instantaneous, local value of the Reynolds number—give better performance than results based on constant values of k_3 determined from initial steady flows. This is consistent with discussions of relevant timescales in sections 2.3 and 6.1 herein. Vitkovsky *et al*. also found that best-fit values of k_3 inferred from comparisons of predictions and measurements depend strongly upon the numerical representation of the equations of motion. This

complication, which is strongly supported by Bughazem and Anderson [28], confuses the interpretation of comparisons between experiment and theory. Nevertheless, there is wide agreement that (1) the authors' predicted values of k_3 are reasonable and (2) the authors' prediction that k_3 should decrease with increasing Reynolds number has been confirmed.

When the above papers were written, comparisons could be made only with predictions from reference [4], not with the revised predictions presented herein. Nevertheless, the papers include qualitative evidence in support of the new weighting function model. First, several of them include statements that the optimum values of k_3 seemed to be somewhat greater than the values of f_{uL} presented in reference [4]. Second — and more important — detailed examination of the *shapes* of the most sudden changes in pressure shows less distortion in the theoretical predictions than in the experimental measurements. Since the effect of unsteady skin friction is highly dissipative, an increase in the value of k_3 would be expected to reduce this difference.

8. CONCLUSIONS

1. A model of transient, turbulent skin friction in smooth-walled pipes has been developed using an idealized representation of the viscosity distribution in the cross-section. The model may be used for any turbulent Reynolds number up to 10^8 and it could be extended easily to higher Reynolds numbers if required.
2. The idealized viscosity distribution has two regions, namely an outer annulus and an inner core. In the outer region, the viscosity is assumed to vary linearly from the laminar value at the wall to a maximum of ν_c at the interface with the core. In the core, the viscosity is uniform and equal to ν_c. This representation has been justified by comparison with experimental data for steady flows (see Figure 1).
3. In both regions of flow, the viscosity is assumed to remain constant throughout short periods of transient flow that are the focus of attention. This simplification has been justified by reference to experimental and theoretical studies. It is not valid for long periods.
4. The method has led to the quantification of turbulent-flow weighting functions that mirror the laminar-flow weighting function introduced by Zielke [5]. In contrast with the laminar-flow case, however, the turbulent-flow weighting function has been shown to vary with the Reynolds number. Another important difference is that the result is expressed in analytical form, valid for the whole range of t.
5. The method has been used to predict theoretical values for a coefficient used in a popular alternative model of unsteady skin friction where the unsteady component of the wall shear stress is assumed to be proportional to the instantaneous acceleration.
6. The predictions have demonstrated that a previous version of the model [6] underestimates the amplitudes of unsteady shear stresses (see Figure 8). Furthermore, it underestimates the lengths of time over which the flow memory can influence current conditions (see Figure 9). The previous model used a uniform *velocity* core, not a uniform *viscosity* core.

REFERENCES

1. J. W. Daily, W. L. Hankey, R. W. Olive and J. M. Jordan 1956 *Transactions of the American Society of Mechanical Engineers* **78**, 1071–1077. Resistance coefficients for accelerated and decelerated flows through smooth tubes and orifices.

2. M. R. Carstens and J. E. Roller 1959 *Journal of the Hydraulics Division, American Society of Civil Engineers* **85**, 67–81. Boundary-shear stress in unsteady turbulent pipe flow.
3. B. Brunone, M. Ferrante and F. Calabresi 2001 4*th International Conference on Water Pipeline Systems, York, UK,* BHR Group. High Reynolds number transients in a pump rising main. Field tests and numerical modelling.
4. A. E. Vardy and J. M. B. Brown 1996 7*th International Conference on Pressure Surges and Fluid Transients in Pipelines and Open Channels, Harrogate, UK*, BHR Group, 289–311. On turbulent, unsteady, smooth pipe friction.
5. W. Zielke 1968 *Journal of Basic Engineering, American Society of Mechanical Engineers* **90**, 109–115. Frequency-dependent friction in transient pipe flow.
6. A. E. Vardy and J. M. B. Brown 1995 *Journal of Hydraulic Research* **33**, 435–456. Transient turbulent, smooth pipe friction.
7. D. H. Axworthy, M. Ghidaoui and D.A. McInnes 2000 *Journal of Hydraulic Engineering, American Society of Civil Engineers* **126**, 276–287. Extended thermodynamics derivation of energy dissipation in unsteady pipe flow.
8. M. Ohmi, S. Kyomen and T. Usui 1985 *Bulletin of the Japanese Society of Mechanical Engineers* **28**, 799–806. Numerical analysis of transient turbulent flow in a liquid line.
9. P. Eichinger and G. Lein 1992 *International Conference on Unsteady Flow and Fluid Transients Durham UK, HR Wallingford*, 41–50. The influence of friction on unsteady pipe flow.
10. B. Brunone, U. M. Golia and M. Greco 1995 *Journal of Hydraulic Engineering, American Society of Civil Engineers* **121**, 906–912. Effects of two-dimensionality on pipe transients modelling.
11. W. F. Silva-Araya and M. H. Chaudhry 1997 *Journal of Hydraulic Engineering, American Society of Civil Engineers* **123**, 108–115. Computation of energy dissipation in transient flow.
12. G. Pezzinga 2000 *Journal of Hydraulic Engineering, American Society of Civil Engineers* **126**, 778–785. Evaluation of unsteady flow resistances by quasi-2D or 1D models.
13. J. Laufer 1954 *NACA TR*1174*, USA*. The structure of turbulence in fully developed pipe flow.
14. M. Ohmi and T. Usui 1976 *Bulletin of the Japanese Society of Mechanical Engineers* **19**, 307–313. Pressure and velocity distribution in pulsating turbulent pipe flow. Part I: Theoretical treatments.
15. S. He and J. D. Jackson 2000 *Journal of Fluid Mechanics* **408**, 1–38. A study of turbulence under conditions of transient flow in a pipe.
16. T. Maruyama, T. Kuribayashi and T. Mizushima 1976 *Journal of Chemical Engineering of Japan* **9**, 431–439. The structure of the turbulence in transient pipe flows.
17. M. S. Ghidaoui, G. S. Mansour and M. Zhao 2002 *Journal of Hydraulic Engineering, of American Society of Civil Engineers* (under review). Analysis of quasi-two-dimensional waterhammer models.
18. E. L. Holmboe and W. T. Rouleau 1967 *Journal of Basic Engineering, American Society of Mechanical Engineers* **89**, 174–180. The effect of viscous shear on transients in liquid lines.
19. B. Brunone, U. M. Golia and M. Greco 1991 9*th Round Table IAHR Group, Valencia*, 273–280. Modelling of fast transients by numerical methods.
20. M. Abramowitz and I. A. Stegun 1965. *Handbook of Mathematical Functions*. New York: Dover.
21. H. Arlt 1983 *Mitteilung Nr.* 102*, Institut für Wasserbau und Wasserwirtshaft, Technische Universität Berlin.* Experimentelle Untersuchungen über das instationäre, turbulente Reibungsverhalten bei aufgeprägten Druckimpulsen in einer Rohrleitung mit Kreisquerschnitt.
22. M. S. Ghidaoui and S. Mansour 2002 *Journal of Hydraulic Engineering, American Society of Civil Engineers* **128**, 102–112. Efficient treatment of the Vardy–Brown unsteady shear in pipe transients.
23. G. Pezzinga 1999 *Journal of Hydraulic Engineering*, *American Society of Civil Engineers* **125**, 676–685. Quasi-2D model for unsteady flow in pipe networks.
24. Z. Zarzycki 1997 3*rd International Conference on Water Pipeline Systems, The Hague, BHR Group,* 163–178. Hydraulic resistance of unsteady turbulent liquid flow in pipes.
25. Z. Zarzycki 2000 8*th International Conference on Pressure Surges, The Hague,* BHR Group, 529–543. On weighting function for wall shear stress during unsteady turbulent pipe flow.
26. A. Bergant, A. R. Simpson and J. Vitkovsky 2001 *Journal of Hydraulic Research* **39**, 249–257. Developments in unsteady pipe flow friction modelling.

27. J. VITKOVSKY, M. LAMBERT, A. SIMPSON and A. BERGANT 2000 8*th International Conference on Pressure Surges, The Hague,* BHR Group, 471–482. Advances in unsteady friction modelling in transient pipe flow.
28. M.B. BUGHAZEM, A. ANDERSON 2000 8*th International Conference on Pressure Surges, The Hague,* BHR Group, 483–498. Investigation of an unsteady friction model for waterhammer and column separation.

APPENDIX A: VELOCITY AND SHEAR IN TRANSIENT FLOW

The method used to derive velocity profiles and shear stresses is described in outline form in sections 3–5. The detailed development for unsteady flows is presented in this appendix and the corresponding development for steady flows is given in Appendix B. In both cases, conditions in the annulus and in the core are first treated independently and are then combined.

A.1. PLANE ANNULUS REGION (LINEARLY VARYING VISCOSITY)

The Laplace transform of equation (5), after substitution of the viscosity distribution in equation (1), may be expressed as

$$(1+\alpha y)\frac{\mathrm{d}^2u'}{\mathrm{d}y}+\alpha\frac{\mathrm{d}u'}{\mathrm{d}y}-\frac{s}{v_w}u'=\frac{P'}{v_w}. \tag{A1}$$

Making the substitution

$$\eta\equiv\frac{2}{\alpha}\sqrt{\frac{s}{v_w}[1+\alpha y]}, \tag{A2}$$

we obtain

$$\frac{\mathrm{d}^2u'}{\mathrm{d}\eta^2}+\frac{1}{\eta}\frac{\mathrm{d}u'}{\mathrm{d}\eta}-u'=\frac{P'}{s}. \tag{A3}$$

The corresponding homogeneous equation has the form of the modified Bessel's equation and so the general solution to the non-homogeneous equation (A3) is

$$u'(\eta)=A_1\mathrm{I}_0(\eta)+A_2\mathrm{K}_0(\eta)-P'/s, \tag{A4}$$

in which A_1 and A_2 are constants of integration to be determined from the boundary conditions and I_0 and K_0 are modified Bessel functions of the first and second kinds and zero order.

The transforms of the boundary conditions in equation (8) are

$$(u')_{y=0}=0,\qquad (u')_{y=b}=u'_{MA}. \tag{A5}$$

Using the substitution in equation (A2), these become

$$u'(\sqrt{\zeta})=0,\qquad u'(\sqrt{\sigma_c\zeta})=u'_{MA}, \tag{A6}$$

in which

$$\zeta\equiv 4s/v_w\alpha^2=[(\eta)_{y=0}]^2. \tag{A7}$$

With these boundary conditions, the constants of integration in equation (A4) are

$$A_1 = -\frac{1}{\Delta}\left[(\mathrm{K}_0(\sqrt{\zeta}) - \mathrm{K}_0(\sqrt{\sigma_c\zeta}))\frac{P'}{s} + \mathrm{K}_0(\sqrt{\zeta})u'_{MA}\right] \tag{A8}$$

and

$$A_2 = -\frac{1}{\Delta}\left[(\mathrm{I}_0(\sqrt{\sigma_c\zeta}) - \mathrm{I}_0(\sqrt{\zeta}))\frac{P'}{s} - \mathrm{I}_0(\sqrt{\zeta})u'_{MA}\right] \tag{A9}$$

in which

$$\Delta \equiv \mathrm{I}_0(\sqrt{\zeta})\mathrm{K}_0(\sqrt{\sigma_c\zeta}) - \mathrm{K}_0(\sqrt{\zeta})\mathrm{I}_0(\sqrt{\sigma_c\zeta}). \tag{A10}$$

It is convenient to decompose these expressions to reflect the dependence of the velocity on the separate contributions of P'/s and u'_{MA}. That is, A_1 and A_2 are expressed as

$$A_1 = A_3(P'/s) + A_5u'_{MA}, \quad A_2 = A_4(P'/s) + A_6u'_{MA}, \tag{A11}$$

in which A_3, A_4, A_5 and A_6 can be deduced by direct comparison with equations (A8) and (A9). With this notation, the velocity distribution in the annulus is

$$u'(\eta) = [A_3\mathrm{I}_0(\eta) + A_4\mathrm{K}_0(\eta) - 1](P'/s) + [A_5\mathrm{I}_0(\eta) + A_6\mathrm{K}_0(\eta)]u'_{MA}. \tag{A12}$$

A.2. CORE REGION (UNIFORM VISCOSITY)

The viscosity in the core region is uniform and equal to v_c. The flow is assumed to be axi symmetric and is modelled using cylindrical polar co-ordinates. The Laplace transform of equation (6) is

$$\frac{1}{r}\frac{\mathrm{d}}{\mathrm{d}r}\left(r\frac{\mathrm{d}u'}{\mathrm{d}r}\right) - \frac{s}{v_c}u' = \frac{P'}{v_c}. \tag{A13}$$

In common with equation (A3), the homogeneous form of this equation is the modified Bessel's equation and so the general solution of equation (A13) is

$$u'(r) = B_1\mathrm{I}_0(r\sqrt{s/v_c}) + B_2\mathrm{K}_0(r\sqrt{s/v_c}) - \frac{P'}{s}, \tag{A14}$$

where B_1 and B_2 are constants of integration to be determined from the boundary conditions given in equation (8). The transform of these is

$$(\mathrm{d}u'/\mathrm{d}r)_{r=0} = 0, \qquad (u')_{r=r_M} = u'_{MC}. \tag{A15}$$

where $r_M = R - b$. With these boundary conditions, the constants of integration in equation (A14) are

$$B_1 = \frac{(u'_{MC} + P'/s)}{\mathrm{I}_0(r_M\sqrt{s/v_c})}, \qquad B_2 = 0, \tag{A16}$$

and the general solution of equation (A13) is

$$u'(r) = \frac{(u'_{MC} + P'/s)\mathrm{I}_0(r\sqrt{s/v_c})}{\mathrm{I}_0(r_M\sqrt{s/v_c})} - \frac{P'}{s}. \tag{A17}$$

A.3. CONTINUOUS VELOCITY PROFILE

A continuous velocity profile across the whole cross-section is obtained by imposing the matching conditions in equation (9). On substituting these into the velocity distributions in the two regions (equations (A12) and (A17)), the transformed velocity at the interface is found to be

$$u'_M = H\left(\frac{P'}{s}\right), \tag{A18}$$

where

$$H \equiv -\frac{M(r_M\sqrt{s/v_c}) + A_3\mathrm{I}_1(\sqrt{\sigma_c\zeta}) - A_4\mathrm{K}_1(\sqrt{\sigma_c\zeta})}{M(r_M\sqrt{s/v_c}) + A_5\mathrm{I}_1(\sqrt{\sigma_c\zeta}) - A_6\mathrm{K}_1(\sqrt{\sigma_c\zeta})}. \tag{A19}$$

The function $M(z)$ in this expression is introduced for simplicity only. It is defined by

$$M(z) \equiv \mathrm{I}_1(z)/\mathrm{I}_0(z). \tag{A20}$$

Using equation (A18), the velocity distribution in the annulus region (equation (A12)) becomes

$$u'(\eta) = [C_1\mathrm{I}_0(\eta) + C_2\mathrm{K}_0(\eta) - 1](P'/s), \tag{A21}$$

where

$$C_1 = A_3 + A_5H = -\frac{1}{\Delta}\left[\mathrm{K}_0(\sqrt{\zeta})(1+H) - \mathrm{K}_0(\sqrt{\sigma_c\zeta})\right] \tag{A22}$$

and

$$C_2 = A_4 + A_6H = -\frac{1}{\Delta}[\mathrm{I}_0(\sqrt{\sigma_c\zeta}) - \mathrm{I}_0(\sqrt{\zeta})(1+H)]. \tag{A23}$$

Similarly, the corresponding distribution in the core region (equation (A17)) becomes

$$u'(r) = \left[\frac{(1+H)\mathrm{I}_0(r\sqrt{s/v_c})}{\mathrm{I}_0(r_M\sqrt{s/v_c})} - 1\right]\frac{P'}{s}. \tag{A24}$$

A.4. MEAN VELOCITY

The rate of flow in the annulus is obtained in an approximate manner. The mean velocity is assumed to be equal to the mean velocity in the planar co-ordinate system. The rate of flow is then approximated by the product of this mean velocity and the true area of the annulus. That is,

$$\frac{Q'_A}{2\pi(r_M + 0{\cdot}5b)} \approx \int_0^b u'(y)\,\mathrm{d}y = \frac{\alpha v_w}{2s}\left[C_1\eta\mathrm{I}_1(\eta) - C_2\eta\mathrm{K}_1(\eta) - \frac{\eta^2}{2}\right]_{\sqrt{\zeta}}^{\sqrt{\sigma_c\zeta}}\frac{P'}{s}. \tag{A25}$$

The use of this approximation is justified on the following grounds:

(1) the exact integration of the velocity distribution given by equation (A21) would be cumbersome in polar co-ordinates; (2) the velocity distribution has been obtained for planar conditions, but even if it were integrated exactly over the annular region using polar

co-ordinates, the result would be approximate; (3) comparisons of the above expression with results obtained by numerical integration of equation (A21) using polar co-ordinates have shown that the errors are typically smaller than 1%; the consequential errors in the overall mean velocity will be even smaller.

The rate of flow in the core is obtained exactly by integrating equation (A24) to give

$$Q'_c = 2\pi \int_0^{r_M} u'(r) r \, \mathrm{d}r = [2\pi r_M \sqrt{v_c/s}(1+H)[\mathrm{I}_1(r_M\sqrt{s/v_c})]/[\mathrm{I}_0(r_M\sqrt{s/v_c})] - \pi r_M^2]\frac{P'}{s}. \tag{A26}$$

The overall mean velocity transform is the ratio of the total flow rate and the cross-sectional area. It is

$$U' = \frac{Q'_A + Q'_C}{\pi R^2}. \tag{A27}$$

The mean velocity transform U' may now be expressed as a function of P'/s, namely

$$P'/s = GU', \tag{A28}$$

where

$$\frac{1}{G} \equiv (r_M + 0{\cdot}5b)\frac{\alpha v_w}{R^2 s}\left[C_1\eta \mathrm{I}_1(\eta) - C_2\eta \mathrm{K}_1(\eta) - \frac{\eta^2}{2}\right]_{\sqrt{\zeta}}^{\sqrt{\sigma_c\zeta}} + \frac{1}{R^2}[2r_M\sqrt{v_c/s}(1+H)[\mathrm{I}_1(r_M\sqrt{s/v_c})]/[\mathrm{I}_0(r_M\sqrt{s/v_c})] - r_M^2]. \tag{A29}$$

A.5. WALL SHEAR STRESS

The shear stress at any position in the annulus is the product of the local viscosity v and the local velocity gradient $\partial u/\partial y$. Differentiating equation (A21) with respect to y, using equation (1) for the kinematic viscosity, and introducing equation (A28), the transform of the shear stress is

$$\tau'_{xy} = \rho v_w(1+\alpha y)\left(\frac{\sqrt{s/v_w}}{\sqrt{1+\alpha y}}\right)[C_1\mathrm{I}_1(\eta) - C_2\mathrm{K}_1(\eta)]GU'. \tag{A30}$$

At the wall, this reduces to

$$\tau'_w = \rho v_w(\sqrt{s/v_w})[C_1\mathrm{I}_1(\sqrt{\zeta}) - C_2\mathrm{K}_1(\sqrt{\zeta})]GU'. \tag{A31}$$

APPENDIX B: VELOCITY AND SHEAR IN STEADY FLOW

In this appendix, the velocity profiles and shear stresses in a steady flow are developed in a similar manner to that used in Appendix A for general flows. The two appendices use the same representation of the viscosity distribution and so the steady-flow results may be regarded as a special case of the general case. As a consequence, differences between the two results may be regarded as indicative of the contribution of unsteadiness that is the focus of this paper.

An alternative method of obtaining the steady-flow relationships would be by deducing the asymptotic forms of the equations in Appendix A as $s \to 0$. The following direct method is preferred because it is easier to reconcile with physical reasoning.

B.1. PLANE ANNULUS (LINEARLY VARYING VISCOSITY)

When the time derivative vanishes, a combination of equations (1) and (5) may be written as

$$\frac{\mathrm{d}}{\mathrm{d}y}\left(v_w(1+\alpha y)\frac{\mathrm{d}u}{\mathrm{d}y}\right) = P. \tag{B1}$$

This can be integrated directly. Upon using the boundary conditions in equation (8), the resulting velocity distribution is

$$u(y) = \frac{Pb^2}{(\sigma_c - 1)v_w}\left(\frac{y}{b} - \frac{\ln(1+\alpha y)}{\ln\,\sigma_c}\right) + u_{MA,s}\,\frac{\ln(1+\alpha y)}{\ln\,\sigma_c}, \tag{B2}$$

where the suffix s denotes steady-flow conditions.

B.2. CORE REGION (UNIFORM VISCOSITY)

For steady flows, equation (6) reduces to

$$\frac{v_c}{r}\frac{\mathrm{d}}{\mathrm{d}r}\left(r\frac{\mathrm{d}u}{\mathrm{d}r}\right) = P. \tag{B3}$$

On integration, subject to the boundary conditions in equation (8), this gives the velocity distribution

$$u(r) = -\frac{P(r_M^2 - r^2)}{4v_c} + u_{MC,s}. \tag{B4}$$

B.3. CONTINUOUS VELOCITY PROFILE

Upon proceeding as in the general case, a continuous velocity profile is obtained by requiring continuity of the velocity and the shear stress (and hence the velocity gradient) at the interface between the annulus and core regions. The implied velocity at the interface is

$$u_{M,s} = -\frac{Pb^2}{v_w\sigma_1(\sigma_c - 1)}\left[\frac{(\sigma_c - 1)r_M}{2b} + \sigma_c - \sigma_1\right], \tag{B5}$$

where

$$\sigma_1 \equiv (\sigma_c - 1)/\ln\,\sigma_c. \tag{B6}$$

The velocity distributions in the annulus and core regions may be found by substituting equation (B5) into equations (B2) and (B4) respectively.

B.4. MEAN VELOCITY

On integration in the manner described in Appendix A for the general case, the steady flow rates in the two regions are found to be

$$Q_{A,s} = -\frac{2\pi(r_M + b/2)}{\alpha^2 v_w}\left(\left[\frac{r_M}{2} + \frac{\sigma_c}{\alpha}\right](\sigma_c\,\ln\,\sigma_c - \sigma_c + 1) - (\alpha b^2/2)\right)P \tag{B7}$$

and

$$Q_{C,s} = -\frac{\pi r_M^2}{\alpha^2 v_w}\left(\frac{\alpha^2 r_M^2}{8\sigma_c} + (\ln\,\sigma_c)[(\alpha r_M/2) + \sigma_c - \sigma_1]\right)P. \tag{B8}$$

The mean velocity $U_s = (Q_{A,s} + Q_{C,s})/\pi R^2$ may therefore be related to P by

$$P = G_s\ U_s, \tag{B9}$$

where

$$\frac{1}{G_s} \equiv\equiv -\frac{2(r_M + b/2)}{R^2\alpha^2 v_w}\left(\left[\frac{r_M}{2} + \frac{\sigma_c}{\alpha}\right](\sigma_c \ln \sigma_c - \sigma_c + 1) - (\alpha b^2/2)\right) - \frac{r_M^2}{R^2\alpha^2 v_w}\left(\frac{\alpha^2 r_M^2}{8\sigma_c} + (\ln \sigma_c)[(\alpha r_M/2) + \sigma_c - \sigma_1]\right). \tag{B10}$$

B.5. WALL SHEAR STRESS

The wall shear stress is obtained by first differentiating equation (B2) with respect to y and choosing $y = 0$. It may be expressed as

$$\tau_{ws} = -(\rho/\alpha)\left[\frac{\alpha r_M}{2} + \sigma_c - 1\right] G_s\ U_s. \tag{B11}$$

After Laplace Transform, this becomes

$$\tau'_{ws} = -(\rho/\alpha)\left[\frac{\alpha r_M}{2} + \sigma_c - 1\right] G_s\ U'_s. \tag{B12}$$

APPENDIX C: NOMENCLATURE

A	parameter defining the approximate weighting function (equation (20))
$A_1,\ A_2$	constants of integration (annulus region)
$A_3, \ldots, A_6$	composite quantities used in Appendix A
b	thickness of the annular region
B	parameter defining the approximate weighting function (equation (20))
$B_1,\ B_2$	constants of integration (core region)
C^*	shear decay coefficient defined in equation (24)
C_1	composite quantity defined in equation (A22)
C_2	composite quantity defined in equation (A23)
f	skin friction coefficient
G	parameter relating the driving force and the mean velocity (see equation (A29))
H	parameter relating the driving force and the matching velocity (see equation (A19))
I_n	modified Bessel function of first kind and nth order
K_n	modified Bessel function of second kind and nth order
M	function defined in equation (A20)
p	pressure
P	"driving force" defined in equation (7)
Q	volume flow rate
r, θ, x	polar co-ordinates—radial, angular and axial
R	pipe radius
Re	Reynolds number
s	Laplace transform variable
t	time
t^*	integration variable ($\equiv\equiv T - t$)
T	time since the disturbance began
u	fluid velocity in the axial (x) direction
u_*	friction velocity
U	mean velocity in the cross-section
U_0	prescribed acceleration in the cross-section
W	weighting function

x, y	Cartesian co-ordinates—axial and lateral
z	argument of function
Z	body force potential

Greek letters

α	lateral rate of change of viscosity in annulus
Δ	function defined in equation (A10)
ζ	value of η^2 at the wall (see equation (A7))
η	similarity variable (equation (A2))
κ	exponent defined by equation (26)
ν	turbulent viscosity
ρ	fluid density
σ_c	core to wall viscosity ratio
σ_1	function of σ_c defined in equation (B6)
τ_{xy}	shear stress in the annular region
τ_w	shear stress at the pipe wall
Φ_u	function relating mean velocity and unsteady wall shear stress transforms
ψ	non-dimensional time defined in equation (24)

Subscripts

A	annulus
c, C	core region
lam	laminar
L	limiting condition
M	matching condition
s	quasi-steady
T	time
u	unsteady
w	wall
0	asymptotic point

Superscripts

$'$	Laplace-transformed quantity